

## Fermi surface and in-plane anisotropy of the layered organic superconductor $\kappa_L$ -(DMEDO-TSeF)<sub>2</sub>[Au(CN)<sub>4</sub>](THF) with domain structures

Tadashi Kawamoto\*

Department of Organic and Polymeric Materials, Graduate School of Science and Engineering, Tokyo Institute of Technology, O-okayama, Meguro-ku, Tokyo 152-8552, Japan

Takehiko Mori

Department of Chemistry and Materials Science, Graduate School of Science and Engineering, Tokyo Institute of Technology, O-okayama, Meguro-ku, Tokyo 152-8552, Japan

Yamaguchi Takahide and Shinya Uji

National Institute for Materials Science, Tsukuba, Ibaraki 305-0003, Japan

David Graf and James S. Brooks

National High Magnetic Field Laboratory and Department of Physics, Florida State University, Tallahassee, Florida 32310, USA

Takashi Shirahata,<sup>†</sup> Megumi Kibune, Hiroko Yoshino, and Tatsuro Imakubo<sup>‡</sup>

Imakubo Initiative Research Unit, RIKEN, Hirosawa, Wako, Saitama 351-0198, Japan

(Received 6 June 2008; revised manuscript received 26 November 2010; published 28 January 2011)

The Fermi surface of the layered organic superconductor  $\kappa_L$ -(DMEDO-TSeF)<sub>2</sub>[Au(CN)<sub>4</sub>](THF) has been investigated, where DMEDO-TSeF is dimethyl (ethylenedioxy) tetraselenafulvalene. Band-structure calculations show that the fundamental Fermi surface is not circular, but elliptical with an eccentricity of 0.76, leading to a large orbital overlap in the extended Brillouin zone. This symmetry is lowered by a structural phase transition at 209 K at which domains form. The magnetic breakdown orbit is observed in the Shubnikov–de Haas oscillations under the low-field region, consistent with the small energy gap at the zone boundary. The observation of the Shubnikov–de Haas effect shows that the present compound has a clean electronic system despite the domain structures.

DOI: [10.1103/PhysRevB.83.012505](https://doi.org/10.1103/PhysRevB.83.012505)

PACS number(s): 74.70.Kn, 71.18.+y, 74.25.Jb

The  $\kappa$ -type molecular arrangement in Fig. 1 is the basis for the highest  $T_c$  materials among organic superconductors,<sup>1</sup> and has been recognized as an almost ideal two-dimensional system. In the  $\kappa$  structure, the donor molecules form face-to-face and head-to-tail orthogonal dimers, where the dimer pairs are approximately 90° with respect to each other. Recently, a family of  $\kappa$ -type organic superconductors of the form  $\kappa$ -(DMEDO-TSeF)<sub>2</sub>[Au(CN)<sub>4</sub>](Solvent) has been developed.<sup>2,3</sup> With the solvent tetrahydrofuran (THF), we obtain two phases that have the same chemical composition,  $\kappa_L$ - and  $\kappa_H$ -(DMEDO-TSeF)<sub>2</sub>[Au(CN)<sub>4</sub>](THF), as shown in Fig. 1. Most organic superconductors are clean single crystals; the donor molecules and anions are in ordered states.<sup>1</sup> Although the THF molecule of the  $\kappa_H$  phase (onset  $T_c = 4.8$  K) is ordered even at room temperature, THF in the  $\kappa_L$  phase (onset  $T_c = 3.0$  K) is disordered due to mirror symmetry. We have determined the structural phase transition in the  $\kappa_L$  phase; the orthorhombic system ( $Pnma$ ) changes to the monoclinic domain structure with the space group  $P2_1/n11$  below the distortion temperature  $T_d = 209$  K.<sup>4</sup> In other words, the  $b$  axis tilts in the  $bc$  plane in real space [Figs. 1(c) and 1(d)]. The  $\kappa_L$  phase is, to our knowledge, the only organic superconductor with a crystallographic domain structure.

The present paper compares the calculated energy band structure with the experimental results from the Shubnikov–de Haas (SdH) effect. Single crystals were prepared by

electrocrystallization in RIKEN.<sup>2</sup> The energy band structure was calculated on the basis of the extended Hückel method and the tight-binding approximation.<sup>5</sup> The magnetoresistance was measured by the four-probe method along the  $b^*$  axis (the interlayer resistance) with ac current (20–200 nA). The SdH measurements were performed by using a superconducting magnet at the National Institute for Materials Science (NIMS), and high field measurements above 18 T were performed in a resistive magnet at the National High Magnetic Field Laboratory (NHMFL) in Tallahassee.

The calculated transfer integrals at room temperature are  $t_{b1} = -356.8$ ,  $t_{b2} = -231.3$ ,  $t_p = -79.6$ , and  $t_q = 55.8$  meV [Fig. 1(b)].  $|t_{b2}|$  is larger by a factor of  $\sim 3$  than  $|t_p|$ , which comes from the Se atoms in the donor molecule and the large dihedral angle (103.0°) of the donor between dimers; this relation differs from that of  $\kappa$ -(BEDT-TTF)<sub>2</sub>X superconductors having  $|t_{b2}| \sim |t_p|$ ,<sup>6</sup> where BEDT-TTF is bis(ethylenedithio)tetrathiafulvalene and X is an anion. The  $\kappa$ -type conductors are reduced to a triangular lattice of dimers with anisotropic transfers  $t$  and  $t'$  as shown in Fig. 2(a), where  $t = (|t_p| + |t_q|)/2$  and  $t' = |t_{b2}|/2$ .<sup>7</sup> This model gives a square lattice in the  $t'/t = 0$  limit, but a one-dimensional chain in the opposite limit ( $t'/t = \infty$ ). For the  $\kappa$ -(BEDT-TTF)<sub>2</sub>X superconductors,  $t'/t$  is between 0.58 and 1.1,<sup>1</sup> and falls in between the square and triangular lattices. Since  $|t_{b2}| > |t_p|$ , the present compound with  $t'/t = 1.71$  is located in the highly anisotropic triangular lattice region.

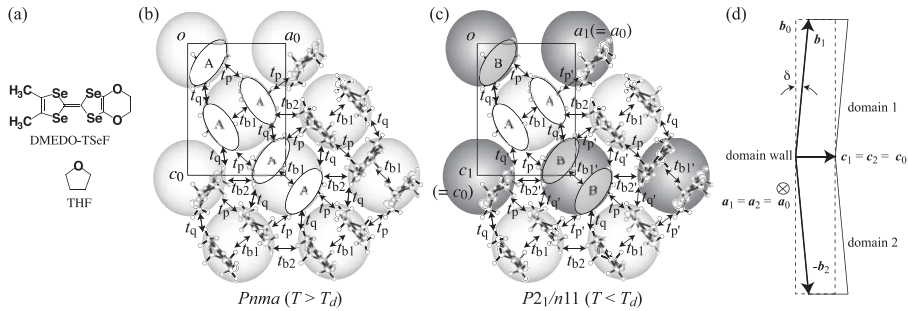


FIG. 1. (a) DMEDO-TSeF and THF molecules. Crystal structure of the  $\kappa_L$  phase projected along the molecular long axis both at (b)  $T > T_d$  and at (c)  $T < T_d$ . Shaded circles in both (b) and (c) represent dimers. (d) Schematic representation of the twinning structure. The domain wall is parallel to the  $ac$  plane of the prototype lattice (i.e., the conducting sheet).

Figure 2(b) shows the calculated energy band structure and Fermi surface at room temperature. In the  $\kappa$ -type compounds, the effective on-site Coulomb repulsion is defined as  $U_{\text{eff}} = 2|t_{b1}|$ .<sup>8</sup> The ratio between  $U_{\text{eff}}$  and the energy bandwidth of the upper band  $W_u$  is  $U_{\text{eff}}/W_u = 0.91$ , indicating a strongly correlated electronic system. The energy bands are degenerate both on the  $X-U$  and  $Z-U$  lines, owing to the crystallographic symmetry. The Fermi surface consists of overlapping cylinders, which generate the fundamental  $\alpha$  and  $\beta$  orbits. The large anisotropy makes the  $\beta$  orbit an elongated ellipse with  $k_{F,c}/k_{F,a} = 1.54$ . As a result, the cross-sectional area of the overlapping  $\alpha$  orbit,  $S_\alpha$ , is 26% of the first Brillouin zone ( $S_{\text{BZ}}$ ), and is considerably larger than the typical value,  $S_\alpha \sim 16\%$  seen experimentally, in the isotropic  $\kappa$ -(BEDT-TTF)<sub>2</sub> $X$  compounds.<sup>6,9</sup> The  $\beta$  orbit,  $S_\beta$ , is exactly the same as  $S_{\text{BZ}}$ .

The degeneracy of the energy bands on the zone boundary occurs when the crystal has glide planes or screw axes having translational symmetry perpendicular to the boundary.<sup>10</sup> Although the low-temperature monoclinic phase of the present compound has  $n$ -glide symmetry that keeps the  $Z-C$  zone boundary degenerate in Fig. 2(c), this symmetry operation creates molecules in another donor layer in the unit cell. The conducting sheet is composed of two independent dimers, giving rise to eight transfer integrals, as shown in Fig. 1(c). Therefore, the energy band splits into two both at the  $X-C$  and at the  $Z-C$  lines, as shown in Fig. 2(c) for the low-temperature

monoclinic phase. As a result, the Fermi surface splits at the  $Z-C$  line, and the  $\beta$  orbit becomes a magnetic breakdown (MB) orbit. We can expect that the value of the energy gap is quite small, because the deviation angle  $\delta = 1.21(2)^\circ$  is extremely small [Fig. 1(d)], and the change of the transfer integrals should be small.<sup>4</sup>

Figure 3(a) is the magnetic field dependence of the electrical resistance at 35 mK ( $B \parallel b^*$ ). Above 15 T, the magnetoresistance shows fast oscillating behavior. The oscillatory part (SdH signal) of the resistance represented by  $[R(B) - R_0(B)]/R_0(B)$ , rescaled by the nonoscillatory background  $R_0(B)$ , is shown in the inset of Fig. 3(a). The fast Fourier transformation (FFT) spectrum based on the SdH signal between 15.2 and 17.8 T shows two peaks  $\alpha$  and  $\beta$  [Fig. 3(b)]. The observed  $S_\alpha$  is 24(2)% of  $S_{\text{BZ}}$ , and that of the  $\beta$  orbit is 103(2)%, where  $S_{\text{BZ}}$  is calculated by using the lattice constants at room temperature. The observed large  $S_\alpha$  verifies the elongated elliptical  $\beta$  orbit.

The observation of the SdH oscillation indicates that the present compound has a clean electronic system despite the domain formation. Since the domain walls are parallel to the conducting sheet [Fig. 1(d)], the domain structure will not affect the cyclotron motion.

In order to investigate the slow oscillating behavior of the background magnetoresistance in Fig. 3(a), we have measured the high field magnetoresistance up to 35 T, as shown in Fig. 4. The small dip structure of the magnetoresistance

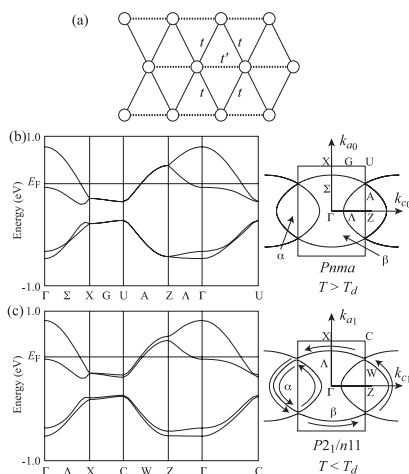


FIG. 2. (a) Dimer model for the  $\kappa$ -type conductors. Open circles represent dimers. Energy band structure and Fermi surface (b) at room temperature, and (c) at  $T < T_d$  using the modified transfer integrals ( $t'_{b1} = 1.1t_{b1}$ ,  $t'_{b2} = 1.1t_{b2}$ ,  $t'_p = 0.9t_p$ , and  $t'_q = 0.9t_q$ ).

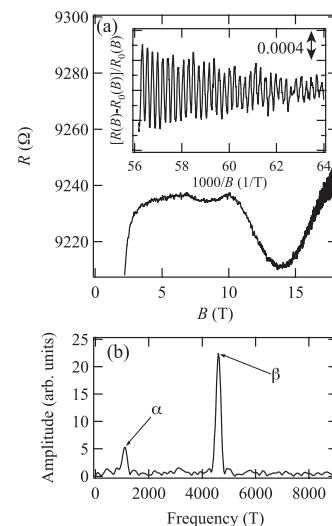


FIG. 3. (a) Magnetoresistance at 35 mK ( $B \parallel b^*$ ). The inset is the SdH signal. (b) FFT spectrum of the SdH oscillation.

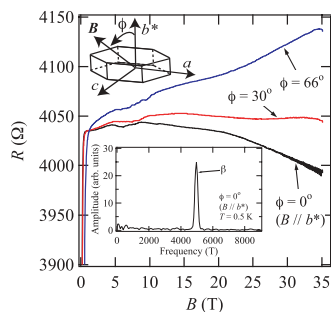


FIG. 4. (Color online) Magnetoresistance at 0.5 K for different field directions. The inset is the FFT spectrum of the SdH oscillation between 26.3 and 35.1 T for  $B \parallel b^*$ . The sample is different from that presented in the other figures.

around 8 T in Fig. 3(a) is found in Fig. 4. However, the second dip structure around 14 T is not found in Fig. 4. Therefore, the slow oscillation like behavior in Fig. 3(a) is not the SdH effect. In the high-field region above 26 T, the SdH oscillation coming from the  $\beta$  orbit is observed, but the  $\alpha$  orbit is not found in the FFT spectrum based on the SdH signal between 26.3 and 35.1 T, as shown in Fig. 4. This indicates that this field region is sufficiently larger than the MB field  $B_0$  related to the energy gap  $E_g$  as  $B_0 \propto E_g^2$ .<sup>1,11,12</sup> Although  $\kappa$ -(BEDT-TTF)<sub>2</sub>Cu(NCS)<sub>2</sub> shows many combination frequencies,  $\beta + n\alpha$  ( $n = -2, -1, 1, 2$ ), under high magnetic field ( $B \geq 20$  T),<sup>13–15</sup> the present compound does not clearly show such orbits.

As shown in Fig. 5(a), the SdH frequencies show  $1/\cos\theta$  behavior as expected for quasi-two-dimensional electronic systems. The frequencies obtained are summarized in Table I with the ratios of the cross-sectional area to the first Brillouin zone. The SdH signals are analyzed in the conventional way by using the two-dimensional Lifshitz-Kosevich (LK) formula for the FFT amplitude

$$A \propto R_T R_D R_s R_b, \quad (1)$$

$$R_T = \frac{K(m^*/m_0)T/(B \cos\theta)}{\sinh[K(m^*/m_0)T/(B \cos\theta)]}, \quad (2)$$

$$R_D = \exp\left(\frac{-K(m^*/m_0)T_D}{B|\cos\theta|}\right), \quad (3)$$

$$R_s = \left|\cos\left(\frac{\pi g^*(m^*/m_0)}{2 \cos\theta}\right)\right|, \quad (4)$$

$$R_b = \exp\left(\frac{-t_i B_0}{2B \cos\theta}\right) \left[1 - \exp\left(\frac{-B_0}{B \cos\theta}\right)\right]^{b_i/2}, \quad (5)$$

where  $m^*$  is the effective cyclotron mass at  $\theta = 0^\circ$ ,  $m_0$  is the free electron mass,  $T_D$  is the Dingle temperature,  $g^*$  is the effective conducting electron  $g$  factor renormalized by many-body effects,  $K$  is equal to  $(2\pi^2 k_B m_0)/(e\hbar) = 14.69$  T/K,  $B_0$  is the magnetic breakdown field, and integers  $t_i$  and  $b_i$  are,

TABLE I. Parameters obtained by the SdH oscillations.

Orbit	$F$ (T)	$S/S_{BZ}$ (%)	$m^*/m_0$	$g^*$	$T_D$ (K)
$\alpha$	$1.1(1) \times 10^3$	24(2)	4.8(4)	1.5(1)	1.7(2)
$\beta$	$4.6(1) \times 10^3$	103(2)	6.3(1)	1.67(3)	2.0–2.5

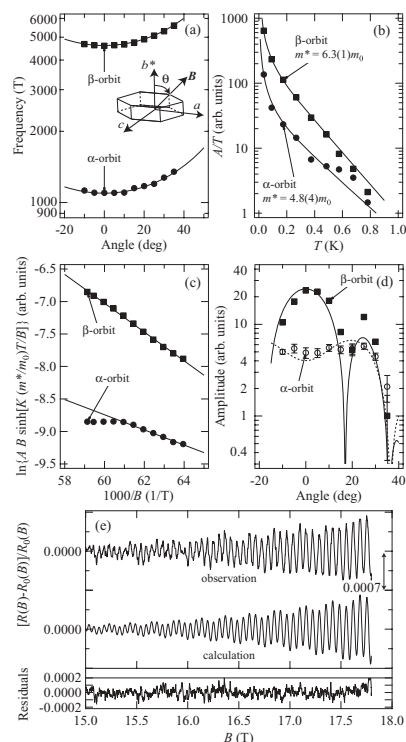


FIG. 5. (a) Angle dependence of the SdH frequencies. Solid lines show the  $1/\cos\theta$  dependence. (b) Mass plots. Solid lines are the fits to the data. (c) Dingle plots. Solid lines are the fits to the data. (d) Angle dependence of the SdH amplitude. Solid and dotted lines are fits to the data. (e) Observed SdH signal (upper) and the calculated signal (lower) with  $B_0 = 4$  T. Residual values are given by the difference between the observed SdH signal and the calculated signal.

respectively, the number of tunneling and Bragg reflections encountered along the path of the quasiparticle.<sup>11,12</sup>

The temperature dependences of the  $\alpha$  and  $\beta$  oscillation amplitudes divided by temperature, mass plots, are presented in Fig. 5(b). The effective cyclotron mass ratios,  $m^*/m_0$ , thus obtained (and listed in Table I) are large among the  $\kappa$ -type organic superconductors.<sup>9</sup>

The probability of the MB tunneling is given by  $P = \exp(-B_0/B)$ .<sup>1,11,12</sup> The coupled network model shows that the amplitude of every term concerned is weighted by a breakdown reduction factor.<sup>16,17</sup> The reduction factor of the  $\alpha$  orbit is  $R_{b,\alpha} = 1 - P = 1 - \exp(-B_0/B)$  from the number of the Bragg reflections ( $t_i = 0$  and  $b_i = 2$ ), and that of the  $\beta$  orbit is  $R_{b,\beta} = P^2 = \exp(-2B_0/B)$  from the number of MB points ( $t_i = 4$  and  $b_i = 0$ ) [Fig. 2(c)]. Therefore, the field dependence of the oscillation amplitude of the  $\alpha$  orbit is proportional to  $A_{0,\alpha} R_{T,\alpha} R_{D,\alpha} R_{b,\alpha}$ , and that of the  $\beta$  orbit is proportional to  $A_{0,\beta} R_{T,\beta} R_{D,\beta} R_{b,\beta}$ , where  $A_{0,\alpha}$  and  $A_{0,\beta}$  are the original oscillation amplitudes of the  $\alpha$  and  $\beta$  orbits, respectively. A fit to the Dingle plot of the  $\alpha$  orbit requires the adjustment of three parameters:  $T_D$ ,  $B_0$ , and the infinite-field intercept  $\ln A_{0,\alpha}$ . Owing to close functional correlations between  $R_D$  and  $R_{b,\alpha}$ , it is virtually impossible to uniquely determine  $T_D$  and  $B_0$  by using the Dingle plots.<sup>14,18</sup> Therefore, we estimate  $T_D$  and  $B_0$  by using the combination of the Dingle plots, the angle dependence of the oscillation amplitude, and the field dependence of the oscillatory magnetoresistance.

Figure 5(c) shows the Dingle plots. The curve of the  $\alpha$  orbit starts to bend down from 16.4 T; this means that the one extreme upper bound of the MB field is  $B_0 \sim 16.4$  T. The Dingle temperature of the  $\alpha$  orbit is estimated as  $T_{D,\alpha} = 1.7(2)$  K by using the slope of the line in the low-field region. This is the lower bound of  $T_{D,\alpha}$ , because the MB occurs in this field region. For the  $\beta$  orbit, the line fitting gives only  $K(m_\beta^*/m_0)T_{D,\beta} + 2B_0 = 222(3)$  T.

The oscillation amplitude of the  $\beta$  orbit shows a drastic decrease at  $\theta \sim 20^\circ$  [Fig. 5(d)]. This decrease is caused by the Zeeman spin splitting damping factor  $R_s$  in the LK formula;  $R_s$  becomes zero when  $(g^*m^*)/(m_0 \cos \theta)$  is an odd integer. For the  $\beta$  orbit,  $g_\beta^* = 1.67(3)$  is smaller than the free electron  $g$  factor; this indicates large renormalization by the many-body effects.<sup>11</sup> For the  $\alpha$  orbit, we treat  $g^*$  and  $B_0$  as the fitting parameters to analyze Fig. 5(d) using Eq. (1). Although the  $\alpha$  orbit behavior is explained by using  $g_\alpha^* = 1.5(1)$ , this angle dependence gives the scattered  $B_0$  between 0.4 and 16.4 T. The Dingle temperature of the  $\beta$  orbit is between 2.0 and 2.5 K under the obtained  $B_0$  region, and this value is reasonable compared with  $T_{D,\alpha} = 1.7(2)$  K.

The oscillatory magnetoresistance at  $\theta = 0^\circ$  is expressed by using

$$\frac{R(B) - R_0(B)}{R_0(B)} = \sum_j A_j \sin \left[ 2\pi \left( \frac{F_j}{B} - \psi_j \right) \right], \quad (6)$$

where  $F_j$  and  $\psi_j$  are the frequency and the phase factor, respectively, of the Fourier component linked to the  $j$  orbit, and the amplitude  $A_j$  is given by  $A_j = A_{0,j} R_{T,j} R_{D,j} R_{s,j} R_{b,j}$ . It is difficult to uniquely determine  $B_0$  using this equation, because

a fit to the field dependence of the oscillation requires the adjustment of parameters:  $B_0$ ,  $A_j$ , and  $\psi_j$ . Figure 5(e) shows the observed SdH oscillation and the calculated result using Eq. (6) with the MB field  $B_0 = 4$  T, and the residual values are not sensitive to the value of  $B_0$ .

The cyclotron motion of the  $\alpha$  orbit disappears for  $B \gg B_0$ , and our estimation satisfies this requirement at  $B \sim 30$  T (Fig. 4). Although several groups have estimated  $B_0$  for  $\kappa$ -(BEDT-TTF)<sub>2</sub>Cu(NCS)<sub>2</sub>, the values of  $B_0$  are scattered between 15 and 41 T.<sup>13–15,19,20</sup> This indicates the difficulty of the estimation of  $B_0$ .

In summary, the large area  $\alpha$  orbit observed in the SdH oscillations shows that the present compound is located in the highly anisotropic triangular lattice regime. The observation of the SdH oscillation near  $B \parallel b^*$  indicates a clean electronic system in the present compound despite the domain structures.

This work was partially supported by Grants-in-Aid for Scientific Research on Innovative Areas (No. 21110511) from the Ministry of Education, Culture, Sports, Science and Technology (MEXT), and the Japan Society for the Promotion of Science (JSPS) Core-to-Core Program (No. 18003). The high-field work above 18 T was made possible through the National Science Foundation (NSF) Cooperative Agreements No. DMR-0084713 (NHMFL), No. DMR-0602859 (J.S.B. Group), the State of Florida, and the US Department of Energy (DOE). One of the authors (T.K.) acknowledges H. Cui and T. Tokumoto for assistance in NHMFL, Tallahassee.

\*kawamoto@o.cc.titech.ac.jp

†Present address: Department of Applied Chemistry, Ehime University, Ehime 790-8557, Japan.

‡Present address: Department of Materials Science and Technology, Nagaoka University of Technology, Niigata 940-2188, Japan.

<sup>1</sup>For a review, see N. Toyota, M. Lang, and J. Muller, *Low-Dimensional Molecular Metals* (Springer, Berlin, 2007).

<sup>2</sup>T. Shirahata, M. Kibune, and T. Imakubo, *Chem. Commun.* (2006), 1592.

<sup>3</sup>T. Shirahata, M. Kibune, H. Yoshino, and T. Imakubo, *Chem. Eur. J.* **13**, 7619 (2007).

<sup>4</sup>T. Kawamoto, T. Mori, T. Kakiuchi, H. Sawa, T. Shirahata, M. Kibune, H. Yoshino, and T. Imakubo, *Phys. Rev. B* **76**, 134517 (2007).

<sup>5</sup>T. Mori, A. Kobayashi, Y. Sasaki, H. Kobayashi, G. Saito, and H. Inokuchi, *Bull. Chem. Soc. Jpn.* **57**, 627 (1984). The atomic orbital parameters we used are in T. Mori and M. Katsuhara, *J. Phys. Soc. Jpn.* **71**, 826 (2002).

<sup>6</sup>For a review, see T. Mori, H. Mori, and S. Tanaka, *Bull. Chem. Soc. Jpn.* **72**, 179 (1999).

<sup>7</sup>M. Tamura, H. Tajima, K. Yakushi, H. Kuroda, A. Kobayashi, R. Kato, and H. Kobayashi, *J. Phys. Soc. Jpn.* **60**, 3861 (1991).

<sup>8</sup>K. Kanoda, *Hyperfine Interact.* **104**, 235 (1997).

<sup>9</sup>T. Kawamoto and T. Mori, *Phys. Rev. B* **74**, 212502 (2006).

<sup>10</sup>G. Burns, *Introduction to Group Theory with Applications* (Academic, New York, 1977).

<sup>11</sup>D. Shoenberg, *Magnetic Oscillations in Metals* (Cambridge University Press, Cambridge, England, 1984).

<sup>12</sup>J. Wosnitzer, *Fermi Surfaces of Low Dimensional Organic Metals and Superconductors* (Springer, Berlin, 1996).

<sup>13</sup>F. A. Meyer, E. Steep, W. Biberacher, P. Christ, A. Lerf, A. G. M. Jansen, W. Joss, P. Wyder, and K. Andres, *Europhys. Lett.* **32**, 681 (1995).

<sup>14</sup>N. Harrison, J. Caulfield, J. Singleton, P. H. P. Reinders, F. Herlach, W. Hayes, M. Kurmoo, and P. Day, *J. Phys.: Condens. Matter* **8**, 5415 (1996).

<sup>15</sup>S. Uji, M. Chaparala, S. Hill, P. S. Sandhu, J. Qualls, L. Seger, and J. S. Brooks, *Synth. Met.* **85**, 1573 (1997).

<sup>16</sup>A. B. Pippard, *Prog. R. Soc. London, Ser. A* **287**, 165 (1965).

<sup>17</sup>L. M. Faalicov and H. Stachowiak, *Phys. Rev.* **147**, 505 (1966).

<sup>18</sup>D. Vignolles, A. Audouard, V. N. Laukhin, J. Béard, E. Canadell, N. G. Spitsina, and E. B. Yagubskii, *Eur. Phys. J. B* **55**, 383 (2007).

<sup>19</sup>T. Sasaki, H. Sato, and N. Toyota, *Physica C* **185**, 2687 (1991).

<sup>20</sup>J. Caulfield, W. Lubczynski, F. L. Pratt, J. Singleton, D. Y. K. Ko, W. Hayes, M. Kurmoo, and P. Day, *J. Phys.: Condens. Matter* **6**, 2911 (1994).